Published in final edited form as:
Neuroinformatics. 2013 January ; 11(1): 119–133. doi:10.1007/s12021-012-9169-7.

Resting State fMRI-guided Fiber Clustering: Methods and Applications

Bao Ge[1], **Lei Guo**[1], **Tuo Zhang**[1,2], **Xintao Hu**[1], **Junwei Han**[1], and **Tianming Liu, Ph.D.**[2,3]
[1]School of Automation, Northwestern Polytechnic University, Xian, China
[2]Bioimaging Research Center, The University of Georgia, Athens, GA
[3]Department of Computer Science, The University of Georgia, Athens, GA

Abstract

Clustering streamline fibers derived from diffusion tensor imaging (DTI) data into functionally meaningful bundles with group-wise correspondences across individuals and populations has been a fundamental step for tract-based analysis of white matter integrity and brain connectivity modeling. Many approaches of fiber clustering reported in the literature so far used geometric and/or anatomic information derived from structural MRI and/or DTI data only. In this paper, we take a novel, alternative multimodal approach of combining resting state fMRI (rsfMRI) and DTI data, and propose to use functional coherence as the criterion to guide the clustering of fibers derived from DTI tractography. Specifically, the functional coherence between two streamline fibers is defined as their rsfMRI time series' correlations, and the affinity propagation (AP) algorithm is used to cluster DTI-derived streamline fibers into bundles. Currently, we use the corpus callosum (CC) fibers, which are the largest fiber bundle in the brain, as a test-bed for methodology development and validation. Our experimental results have shown that the proposed rsfMRI-guided fiber clustering method can achieve functionally *homogeneous* bundles that are *reasonably* consistent across individuals and populations, suggesting the close relationship between structural connectivity and brain function. The clustered fiber bundles were evaluated and validated via the benchmark data provided by task-based fMRI, via reproducibility studies, and via comparison with other methods. Finally, we have applied the proposed framework on a multimodal rsfMRI/DTI dataset of schizophrenia (SZ) and *reproducible* results were obtained.

Keywords

Resting state fMRI; DTI; fiber clustering; tract-based analysis

1. Introduction

Diffusion tensor imaging (DTI), as a powerful tool to image the axonal fibers in vivo (Basser and Pierpaoli, 1996; Mori et al., 1999; Basser et al., 2000; Westin et al., 2002; Mori 2006), provides rich structural connectivity information that has been demonstrated to be closely related to brain function (e.g., Behrens et al., 2003; Behrens et al., 2004; Skudlarski et al., 2008; Honey et al., 2009; Zhang et al., 2011;). In order to infer meaningful and comparable information from DTI data of different brains, the large number of fiber

*To whom correspondence should be addressed: Tianming Liu, Assistant Professor, Department of Computer Science & Bioimaging Research Center, The University of Georgia, Boyd GSRC 420, Athens, GA 30602, Phone 706-542-3478, tliu@uga.edu, Web: http://www.cs.uga.edu/~tliu.

Information Sharing Statement: Source codes of the proposed computational algorithms and methods are available at: http://www.cs.uga.edu/~tliu/neuroinformatics/neuroinformatics_fiberclustering.rar.

trajectories produced by streamline DTI tractography (Mori et al., 1999; Westin et al., 2002) need to be grouped into appropriate fiber bundles for tract-based analysis (e.g., Brun et al., 2004; Gerig et al., 2004; Maddah et al., 2006; O'Donnell et al., 2006; Li et al., 2010b). Typically, there are two important steps involved in automated white matter fiber clustering. The first step is to define an appropriate similarity measure between fibers, and the second step is to apply clustering methods to generate groups of fibers, such as via spectral clustering (Brun et al., 2004), hierarchical clustering (Gerig et al., 2004; Corouge et al., 2004), expectation-maximization (Maddah et al., 2006), and normalized cut (Brun et al., 2004; O'Donnell et al., 2006). Many previous studies have chosen shapes and/or end point positions (e.g., Maddah et al., 2006; Brun et al., 2004; Corouge et al., 2004; Zhang et al., 2010; Li et al., 2010b) of fibers as the features by which to measure fiber similarity. For example, Maddah et al., (2006) represented fibers as 3D quintic B-splines, Brun et al., (2004) tried to capture the above-mentioned three features using a 9-D descriptor, and Corouge et al., (2004) and Gerig et al., (2004) proposed a variant of Hausdorff distance that contains position and shape information. An alternative method for fiber clustering is the atlas-based approach. For example, Ge et al., (2010) represented fiber by a sequence of atlas labels and clustered fibers using the symbolic sequence analysis method in bioinformatics. Xia et al., (2005) grouped fibers as part of the same bundle if the end points of individual fibers fell within a common region of a gray matter atlas. This idea was further explored in Li et al., 2010b via a hybrid procedure of an atlas-based whole-brain parcellation and shape based fiber clustering. Maddah et al., (2005) constructed an atlas by averaging statistical fiber bundle models, and clustered the fiber tracts based on the atlas. Wakana et al., (2007) used a prior knowledge about fiber bundles and defined one or more region of interest (ROIs) to identify special fiber bundles. These methods have their own advantages and have been successfully used in different applications.

However, there are challenges associated with existing fiber clustering methods. First, in some fiber bundles such as the corpus callosum (CC) (Paul et al., 2007), fiber shapes could be very similar in certain regions and it could be difficult to determine where the boundaries are during fiber clustering based only on fiber shape patterns. Fig. 1(a) illustrates an example of this difficulty. For the fiber end point based clustering method, the whole process is dependent on the annotation of fiber ends, which heavily relies on cortical parcellation and recognition results (Li et al., 2010b). Since cortical parcellation and recognition is still an open problem in the field (Liu et al., 2011), fiber clustering based on fiber end points could be challenging, as illustrated in Fig. 1(b). Second, since many existing methods were based on anatomic and/or geometric information, the functional interpretation of the fiber clustering results is not immediately clear. For instance, boundaries generated in the shape-based fiber clustering procedure are not necessarily corresponding to functionally *homogeneous* bundles (Ge et al., 2011). The above two challenges motivated us to explore novel, alternative function-guided methodologies to perform fiber clustering.

Recently, resting state fMRI (rsfMRI) has been demonstrated to be an effective neuroimaging modality by which to explore the functional networks in the human brain, because similar low-frequency oscillations in rsfMRI time series between spatially distinct brain regions are indicative of correlated functional activity patterns in the brain (e.g., Fox and Raichle, 2007; Cohen et al., 2008; Heuvel et al., 2008; Li et al., 2010). In addition, a variety of recent studies demonstrated that structural connectivity derived from DTI data is closely correlated with the functional connectivity derived from rsfMRI data (e.g., Honey et al., 2009; Skudlarski et al., 2008; Li et al., 2010; Zhang et al., 2011). Inspired by these studies, we are motivated to apply the criterion of functional coherence to cluster white matter fibers based on the premise that the clustered fibers within a bundle should have functional homogeneity. *As far as we know, this work is among the earliest attempts to combine DTI-based fiber clustering with resting state fMRI data*. Our general hypothesis is

that under the guidance of rsfMRI data, the clustered fiber bundles will possess both structural and functional similarities across different brains. To test this hypothesis, we represent a white matter fiber by two rsfMRI time series extracted from the two gray matter (GM) voxels that the fiber's two end points connect, and the functional coherence between white matter fibers is measured by the correlation between their rsfMRI time series (Li et al., 2010). Then, the data-driven affinity propagation (AP) algorithm (Frey and Dueck, 2007) is applied to cluster fibers into bundle tracts. Instead of working on the whole-brain fibers, we currently use the corpus callosum (CC) fibers, which are the largest fiber bundle in the brain (Paul et al., 2007), as a test-bed for algorithm development and validation. Our experimental results using multimodal rsfMRI and DTI datasets show that the proposed rsfMRI-guided fiber clustering method can achieve meaningful fiber bundles. Notably, an early short version of this methodology was presented in the MICCAI 2011 conference (Ge et al., 2011).

2. Materials and Methods

2.1. Overview

As summarized in Fig.2, the algorithmic pipeline includes the following steps. First, we pre-processed the raw DTI data, and then performed brain tissue segmentation (Liu et al., 2006; Liu et al., 2007) and fiber tracking (via MEDINRIA) based on DTI data. At current stage, the well-established streamline tractography approach (Mori et al., 1999; Westin et al., 2002) was used in this paper to develop and validate the rsfMRI-guided fiber clustering methodology. Then, the tracked fiber trajectories were projected to the cortical surface via a similar method in Li et al., 2010 to facilitate the extraction of rsfMRI signals on the gray matter volume, which will be detailed in section 2.3.1. Based on the brain tissue segmentation map, we reconstructed white matter surface via validated in-house toolkits (Liu et al., 2004; Liu et al., 2008; Nie et al., 2011). Also, we registered the rsfMRI images to the DTI space using FSL FLIRT. Afterwards, we clustered fibers into bundles based on the fibers' function coherences via the affinity propagation algorithm (Frey and Dueck, 2007). We displayed clustered fiber bundles on reconstructed cortical surfaces and semi-automatically identified 16 consistent fiber bundles from a group of subjects for evaluation and validation. The reproducibility of the proposed method was evaluated by repeated scans of rsfMRI datasets, and its performance was compared with other shape based methods in section 3.3. In particular, part of the clustered bundles was validated via the benchmark data provided by task-based fMRI (Faraco, et al., 2011). Finally, we compare the DTI-derived measurements of fractional anisotropy (FA) and mean diffusivity (MD) for the clustered fiber bundles between schizophrenia (SZ) patients (Zhang et al., 2011b) and matched normal controls. Experimental results demonstrate that SZ patients have decreased MD and increased FA values in some clustered bundles in the CC.

2.2. Multimodal data and pre-processing

Seven volunteers were scanned using a 3T GE Signa MRI system at the Bioimaging Research Center (BIRC) of The University of Georgia. We acquired the rsfMRI data with dimensionality 128*128*60*100, space resolution 2mm*2mm*2mm, TR=5s, TE=25 ms, and flip angle 90 degrees (Li et al., 2010). DTI data was acquired using the same spatial resolution as the rsfMRI data; parameters were TR=15.5 s and TE=89.5 ms, with 30 DWI gradient directions and 3 B0 volumes acquired. For three out of the seven subjects, the working memory OSPAN tasks (Faraco et al., 2011) was used for fMRI data acquisition with the parameters of 64×64 matrix, 4 mm slice thickness, 220mm^2 FOV, 30 slices, TR=1.5 s, TE=25 ms, ASSET=2. Pre-processing of the rsfMRI data included brain skull removal, motion correction, spatial smoothing, temporal pre-whitening, slice time correction, global drift removal, and band pass filtering (0.01Hz∼0.1Hz) (Li et al., 2010).

For the DTI data, pre-processing included brain skull removal, motion correction, and eddy current correction (Liu et al., 2006; Liu et al., 2007). After the pre-processing, *the whole brain's fiber tracking* was performed using MEDINRIA (FA threshold: 0.2; minimum fiber length: 20), *and the corpus callosum fibers were selected by manually defined ROIs*. Based on pre-processed DTI data, brain tissue segmentation was performed using the multi-channel fusion method akin to that in Liu et al., 2007, and then the cortical surface was reconstructed via the approach in Liu et al., 2008. DTI space was used as the standard space from which to generate the tissue segmentation and from which to exhibit the functional coherent fiber bundles on the cortical surface. Also, DTI and fMRI images were registered via FSL FLIRT. Since both rsfMRI and DTI images use both EPI (echo planar imaging) sequences, their distortions tend to be similar (Li et al., 2010). Importantly, our prior studies have demonstrated that the misalignment between DTI and fMRI images is much less than that between T1-weighted MRI and fMRI images (Li et al., 2010).

2.3. Fiber clustering based on functional coherence

In general, we compute the functional correlation of the GM voxels' rsfMRI signals located on the fiber ends as the similarity between any pair of fibers, and then apply the affinity propagation algorithm (Frey and Dueck, 2007) to cluster fibers into bundles.

2.3.1. Extraction of rsfMRI signals from a fiber's two ends

It should be noted that the blood supply to the white matter is significantly lower than that of the cerebral cortex (less than one fourth) (Mezer, et al., 2009), and the blood-oxygen-level dependence (BOLD) contribution of the white matter is relatively low. Hence, the investigation of gray matter (GM) rsfMRI signals is more reasonable. Therefore, before extracting rsfMRI signals from GM voxels for a fiber's two ends, we project some fibers into the gray matter cortex since the DTI-derived fiber trajectories are not necessarily located on the cortex due to two reasons. 1) DTI fiber tractography using the streamline approach has difficulty in tracking inside GM since the FA (fractional anisotropy) values around the boundaries of gray matter and white matter are relatively low. As a result, there are some fibers that cannot reach the GM. 2) There is discrepancy in brain tissue segmentation based on DTI data and the DTI tractography (Liu et al., 2006; Liu et al., 2007). In this case, the fiber could be either outside the cortex if the GM is over-segmented, or inside the cortex if the GM is under-segmented.

In order to make use of the fiber connection information on the cortex, we projected the fibers onto the cortical surface guided by the tissue segmentation map. There are four types of fiber projections here. 1) If the end point of a fiber already lies on a GM voxel in the brain tissue map, no search is conducted, e.g., fiber #1 shown in Fig. 3(a); 2) If the end point of a fiber lies inside the cortex, e.g., the fiber #2 shown in Fig. 3(a), we search forward along the tangent direction until reaching the gray matter. 3) Otherwise, e.g., the fiber #3 shown in Fig. 3(a), we search backward along the tangent direction until reaching the gray matter. The search process stops either when the fiber arrives at a GM voxel or it exceeds a search threshold. 4) In very rare cases when a fiber cannot reach the surface, e.g., the fiber #4 shown in Fig. 3(a), we treat this fiber as an outlier and remove it from the data. Fig. 3(b) shows the positions that the fibers arrive at after the projection. The search was conducted iteratively until at least one GM voxel can be found in the 1-ring surface vertex neighborhood of the current seed point, or the number of iteration exceeds a given threshold. Notably, we experimentally chose the threshold value for the iteration number. In general, the iteration number for those #2 or #3 fibers that can be projected to the GM voxels is stable within a reasonably range of the threshold value (e.g., from 3 to 9 in this work). Furthermore, the projection step can guarantee that almost all #3 and #2 fibers can arrive at GM voxels after this range of iterations. When multiple GM voxels exist, the closest one is

used as the projected point. Finally, for each projected fiber, we extract the rsfMRI signals for its two ends. Fig. 3(c) shows the histogram of the four types of fiber, from which we can see that type 1 accounts for about 40% of fibers (these fibers were preserved), type 2 and type 3 account for about 50% (these were extended or pruned), and the remaining 10% of fibers were eliminated.

2.3.2. Measurement of functional coherence among fibers

As illustrated in Figs. 4(a)-Figs. 4(c), given any pair of fibers with four end points located in the gray matter, the functional coherence between these two fibers is defined as follows:

$$C=0.5^{*}(max(C_{13}, C_{14})+max(C_{23}, C_{24})) \quad (1)$$

where

$$C_{13}=PsCor\,(v1, v3)\,, \qquad C_{14}=PsCor\,(v1, v4)\,,$$
$$C_{23}=PsCor(v2, v3), \qquad C_{24}=\mathrm{PsCor}(v2, v4)$$

Here, *vi* indexes fMRI signal of the end points of two fibers, the function *PsCor* is the Pearson correlation coefficient of the fiber's two end points' rsfMRI signals. If the two fibers are close in space, the correlations C_{13} and C_{24} are typically high, but correlations C_{23} and C_{14} could be low. In fact we do not know which is the fiber's start point or end point, so the Equation (1) will evolve into the following four cases:

Thus, for the first situation, the two fibers will be clustered into the same bundle. For the 2nd and 3rd situations, the two fibers will be probably clustered into the same bundle. For the 4th situation, the two fibers will not be clustered into the same bundle. Our premise here is that the fibers belonging to the same tract should have higher functional coherence, and those belonging to different tracts should have lower coherence. The similarity matrix is ordered in the fiber ID sequence which is color-coded in Fig. 4(d). Then, the functional similarity matrix can be computed, as shown in Fig. 4(e). The color bar for the similarity is on the right-most side. We can visually inspect some potential clusters from the visualization in Fig. 4(e). Afterwards, the affinity propagation algorithm (Frey and Dueck, 2007) is applied on this matrix to automatically cluster the fibers into functionally *coherent* bundles.

It should be noted that the criterion of functional coherence derived from rsfMRI data offers a unique capability to cluster functionally coherent fibers into the same bundle and differentiate non-coherent fibers into different bundles. As an example, Fig. 5(a) shows three fibers that are functionally coherent, and thus they should be clustered into one bundle. However, if we use geometric or shape criteria (Maddah et al., 2006; Gerig et al., 2004; Zhang et al., 2010), e.g., the Euclidean distances between neighboring fibers, the blue fiber in Fig. 5(a) (highlighted by a red arrow) is likely to be separated from the bundle composed of the red and green ones. Another example is shown in Fig. 5(b), in which the blue fiber (highlighted by a red arrow) has low functional coherence with the green and red ones and thus the blue one can be differentiated from other two fibers via rsfMRI data. However, geometry and/or shape based fiber clustering methods are likely to have difficulties in differentiating the blue fiber from other two functionally different fibers. Hence, from these two examples, we can see that the criterion of functional coherence is a powerful approach for fiber clustering. It should also be noted that this paper focuses on the CC fibers (Paul et al., 2007), which typically share similar shape patterns within a neighborhood, and thus only functional coherence derived from rsfMRI data was used for the definition of fiber

similarity. In the future, if other fibers with more complex and variable shape and connectivity patterns such as cortico-cortical and cortical-subcortical pathways are considered, additional geometric or anatomic constraints (Li, et al., 2010b) should be considered in the definition of fiber similarities.

2.3.3. Fiber clustering via the affinity propagation algorithm

The affinity propagation (AP) (Frey and Dueck, 2007) algorithm is an effective algorithm that takes as input measures of similarity between pairs of data points and simultaneously considers all data points as potential exemplars and passes soft information around until a high-quality set of exemplars and corresponding clusters gradually emerges. In the affinity propagation algorithm, each cluster is represented by a data point called a cluster center, or an exemplar, and the method searches for cluster so as to maximize a goal function called net similarity. The inputs are the pair-wise similarities and data point preferences. In this paper, the inputs are the pair-wise fibers' functional coherences. Specifically, the similarity ***s(i,k)*** indicates how well the data point ***k*** is suited to be the exemplar for data point *i*. The preference ***s(i,i)*** is the a priori suitability of point ***i*** to serve as an exemplar. Preferences can be set to a global (shared) value, or customized for particular data points. High values of the preferences will cause affinity propagation to find many exemplars (clusters), while low values will lead to a small number of exemplars (clusters). The number of identified exemplars is affected by both the values of the input preference and the messaging-passing procedure. In this paper, we applied the AP clustering method on the functional similarity matrix of all fibers in the corpus callosum, and achieved the clustered fiber bundles. In particular, each fiber cluster is represented by the fiber exemplar discovered during the AP clustering procedure.

3. Results

3.1. Identification of functionally coherent fiber bundles

Based on the dataset in Section 2.2, the fibers of corpus callosum (CC) were clustered into around 30 bundles for 7 subjects separately, as shown in the 7 rows in Fig. 6(a). For the sake of visual differentiation, each fiber bundle was represented by the fiber exemplar obtained during the affinity propagation clustering procedure, as shown in Fig. 6(b). In order to identify the corresponding fiber bundles in different subjects, first, we registered all the other subjects' B0 images to subject #1 (selected as a template) via the FSL FLIRT. Accordingly, a deformation matrix was generated by which all fiber exemplars were also warped. Then, we computed the Hausdorff distances (Li et al., 2010b) between the representative exemplars across subjects and selected those exemplars that are closest to the representative exemplars in other subjects. Thus, out of 30 clustered exemplars, we visually confirmed 16 most consistent representative exemplar fibers across different subjects, as shown in Fig. 6(c). Each corresponding fiber exemplar in Fig. 6(c) has the same color in different brains. It is evident that the distributions of these 16 fiber exemplars are *reasonably* consistent. Quantitatively, we provided a Hausdorff distance table (Table 1) of the 16 fiber exemplars, which shows the Hausdorff distances between pairs of corresponding fiber exemplars in the subject #1 and those in other subjects. It is evident that the Hausdorff distances are quite low, suggesting the good correspondences of clustered fiber bundles across seven different brains. As another example, Fig. 7 visualizes 16 corresponding bundles from 3 randomly selected subjects. Four fiber bundles are shown in each figure so that we can more easily check the correspondences between fiber bundles in different brains. Each row in Fig. 7 shows that the clustered bundles are reasonably consistent. Therefore, the results in this section have demonstrated that the rsfMRI-guided fiber clustering procedure can achieve consistent CC fiber bundles with functional coherences, suggesting the close relationship between consistent structural connectivity and coherent brain function (Zhang,

et al., 2011). This principle also lays down the neuroscience basis of the proposed rsfMRI-guided fiber clustering methodology.

3.2. Reproducibility

To test the reproducibility of the proposed method, we performed the same clustering process on two repeated scans of rsfMRI data for the same group of subjects, and the clustering results for 3 subjects with repeated rsfMRI scans are shown in Fig. 8. Fig. 8(a) shows all the exemplars, and Fig. 8(b) shows the identified 16 exemplars. For the sake of comparison, the 16 exemplars from the previous clustering result are also shown in Fig. 8(c), which correspond to the #1, #3, #5 rows of Fig. 6(c). By visual examination, we can clearly see that the two clustering results are very similar. Furthermore, the Hausdorff distances between the corresponding fiber exemplars in Fig. 8(b) and Fig. 8(c) are given in Table 2. Some “0” values mean that the two clustering procedures identified exactly the same exemplars. Other corresponding fiber exemplars are also at close positions based on the Hausdorff distances. Therefore, the results in Fig. 8 and Table 2 demonstrate that the proposed rsfMRI-guided fiber clustering procedure is *reasonably* reproducible across repeated rsfMRI scans and across subjects, suggesting the robustness of the proposed method. This result also confirms that rsfMRI-derived functional connectivity is a reliable and reproducible measurement of the functional brain architecture, which has been reported in a variety of publications (e.g., Fox and Raichle, 2007; Cohen et al., 2008; Heuvel et al., 2008; Li et al., 2010).

3.3. Comparison with shape based fiber clustering method

As further evaluations, we compared our method with shape based fiber clustering method. We selected the mean closest distance as the feature, which is a modification of the Hausdorff distance and contains both position and shape information (Corouge et al., 2004; Gerig et al., 2004). The clustering is based on the affinity propagation algorithm. An example is shown in Fig. 9. Fig. 9(a) is the same as the first row in Fig. 6(c), and we selected four fiber exemplars to display their corresponding fiber bundles, as shown in Fig. 9(b). Figs. 9(c) and Figs. 9(d) show the clustered fibers by adopting the mean closest distance as the clustering feature, and there are 7 clustered bundles altogether as shown in Fig. 9(c). For the purpose of comparison, in Fig. 9(d), we visualized those fibers in Fig. 9(b) which overlap with the two clusters of the 7 fiber bundles in Fig. 9(c). Those fibers circled by yellow dotted curves were clustered into 3 fibers bundles by our rsfMRI-guided fiber clustering method, but cannot be differentiated by the shape based method although they are different in terms of functional coherence. This result demonstrated the potential benefit of applying rsfMRI data to guide the clustering of functionally inhomogeneous fibers but with similar geometric shapes or close anatomical trajectories.

3.4. Validation by task-based fMRI data

In addition to the qualitative and quantitate evaluations of the clustered CC fiber bundles in Section 3.1-3.3, we used a working memory task-based fMRI dataset (Faraco et al., 2011) as a benchmark to examine the functional correspondences of the clustered fiber bundles. Specifically, the working memory task-based fMRI data provided 16 consistently activated brain regions, as shown by the white boxes in Fig. 10. These task-based fMRI-derived regions of interests (ROIs) provide the benchmark data for comparison of functional correspondences of fiber bundles. It is interesting that one fiber bundle *(green one in* Fig. 10(a)*)* coincidently falls into the neighborhoods of two corresponding working memory ROIs of left and right paracingulate gyri (highlighted by red arrows) consistently in the testing subjects. The Euclidean distances between the ROI's centers and fiber exemplars are 3 mm, 0.1 mm, 3.9 mm, and 2.8 mm respectively, as shown in Fig. 10(a). These close

vicinities indicate that the paracingulate gyri are consistently connected by the green fiber bundle across individuals, suggesting that the proposed rsfMRI-guided fiber clustering method indeed grouped *this example of* functionally coherent fibers *(represented by the exemplars)* into the same bundle. For further visualization examination, Fig. 10(b) shows two views of the fiber bundles corresponding to the two exemplars in green in Fig. 10(a). This result further confirmed the close relationship between structural connectivity and brain function (Behrens et al., 2003; Behrens et al., 2004; Skudlarski et al., 2008; Honey et al., 2009; Zhang et al., 2011; Zhu et al., 2011), which is the underlying neuroscience principle of the proposed rsfMRI-guided fiber clustering approach.

3.5. Application on schizophrenia dataset

We applied the proposed method to perform tract-based fiber analysis on a multimodal DTI/rsfMRI dataset of schizophrenia (SZ) (Zhang et al., 2011b). 8 SZ patients and 7 healthy control subjects were downloaded from (http://hdl.handle.net/1926/1687) and used for this study. Briefly, DTI scans were acquired on a 3 Tesla GE system using an 8 Channel coil and Array Spatial Sensitivity Encoding Techniques (51 directions with b=900s/mm^2, 8 baseline scans with b=0, TR=17000 ms, TE=78 ms, FOV=24 cm, 144×144 matrix, 1.7 mm slice thickness to cover the whole brain, voxel size 1.67×1.67×1.7 mm^3). Resting state fMRI sequences were acquired with an additional EPI BOLD sequence using 8 Channel coil. It was 10 minutes long, and contains 200 repetitions of a high resolution EPI scan (96×96 in plane, 3mm thickness, TR=3000 ms, TE=30 ms, 39 axial slices, ASSETT). Subjects closed their eyes and rested during rsfMRI scans. More details of preprocessing are referred to Zhang et al., 2011b.

As the largest commissural fiber of the human brain, the corpus callosum (CC) plays a central role in the misconnection models of SZ (e.g., Downhill et al., 2000; Innocenti et al., 2003). A variety of brain imaging studies of SZ (e.g., Kanaan et al., 2005; Kubicki et al., 2007; Kyriakopoulos et al., 2008) focused on the exploration of differences in volume, shape and fiber integrity, but results reported in the literature are inconsistent (Rotarska-Jagiela et al., 2008). By using the proposed method, we clustered the CC fibers into about 30 functionally coherent fiber bundles and the 16 most consistent fiber bundles and exemplars were also selected, as shown in Fig. 11. Each corresponding fiber bundle has the same color in different brains, as shown in SZ (Fig. 11(a)) and control (Fig. 11(b)) groups. It is interesting that these 16 most consistent fiber bundles and exemplars in both SZ and controls are the same as those in our results in Figs. 6-8. This result suggests that our rsfMRI-guided fiber clustering approach can reliably and consistently identify 16 corresponding CC fiber bundles across individuals and populations *via different multimodal DTI and rsfMRI datasets*.

4. Discussion and Conclusion

To achieve the goal of clustering functionally-coherent fiber bundles, this paper presents a novel, alternative methodology of using rsfMRI data to guide fiber clustering. The underlying neuroscience basis is that axonal fibers within a bundle should have functional coherence, and our results have shown that functional coherence is a meaningful criterion for fiber clustering by evaluating its reproducibility and comparing with other methods. The reproducible and consistent fiber clustering results in repeated rsfMRI scans and in two separate multimodal DTI/rsfMRI datasets demonstrated the robustness and effectiveness of the methodology. In particular, part of the clustered bundles was validated via task-based fMRI benchmark data, and our results showed that rsfMRI-guided fiber clustering generated bundles that connect corresponding functional areas in different brains. Furthermore, we applied the method for CC tract-based analysis of schizophrenia, and the experimental result

demonstrated the increase of FA and the decrease of MD in CC fiber bundles of schizophrenic subjects, in comparison with healthy controls.

The results reported in this paper further demonstrated that integration of multimodal DTI and fMRI data could potentially significantly enhance human brain mapping (Zhu et al., 2011; Liu et al., 2011), since the complementary DTI and fMRI data can offer rich structural and functional information about the brain. For instance, functional coherence can be used to constrain the structural connectivity consistency as shown in this paper, or structural connectivity coherence can be used to regulate the localization of functional regions (Zhu et al., 2011; Zhang et al., 2011). However, it should be noted that functionally connected regions do not necessarily always exhibit direct fiber connections. At the current stage, our method is applied on those existing fiber connections, which are grouped into clusters based on functional coherence. In the future, we plan to investigate the intrinsic relationships between structural and functional connections so that they can be better utilized as meaningful constraints in either fiber clustering or functional network inference applications.

The computational pipeline presented in Section 2 can be improved or enhanced in several directions. First, due to the limitation of the DTI's resolution and the tensor model, we need the step of fiber projection before extracting the GM voxel's signal on the fiber's endpoint. In the future, advancements of neuroimaging techniques such as the High Angular Resolution Diffusion Imaging (HARDI) (Tuch et al., 2002) and ultra-high field MRI (Kerchner, 2011), which has higher quality and can effectively deal with crossing white matter fibers, can further enhance the rsfMRI-guided fiber clustering procedure. Second, currently, only CC fibers were used for algorithm development and evaluation purposes in this paper. In the future, we plan to apply the proposed methodology to other major fiber bundles with more complex shape and connectivity patterns such as cortico-cortical and cortical-subcortical pathways so that large-scale rsfMRI-guided fiber clustering can be performed. *Third*, in current rsfMRI-guided fiber clustering procedure, only resting state functional coherence was used as the similarity measurement. This worked well for fibers bundles like CC, but it is not always applicable to the whole brain because two functionally similar fibers may have a large distance. In the future, we will investigate other information such as structural connectivity information and anatomical information to possibly constrain the clustering of those more complex and variable fibers. *Fourth*, the consistent fiber bundles across subjects were difficult to identify. Thus, at the current stage, we achieved this by a Hausdorff distance based semi-automatic technique. In the future, we will examine if it is possible to learn predictive models of fiber bundles from existing clustered and validated clustering results, e.g., via the approach in our recent work in Zhang et al., 2011. If successful, these learned prior models of consistent fiber bundles could be used as additional constraints during the fiber clustering of new subjects with DTI/rsfMRI data.

In addition, the proposed rsfMRI-guided fiber clustering approach will be further evaluated and validated via larger scale datasets. For instance, more task-based fMRI datasets of other functional networks will be used to validate other clustered fiber bundles, in addition to the working memory network used in this paper. The 16 consistent CC fiber bundles obtained in Section 3 will be further replicated in larger scale multimodal DTI/rsfMRI datasets. Once these fiber bundles are confirmed to exhibit both consistent structural and functional properties, they can be used as a common and effective representation of the human brain architecture. Finally, we plan to apply the proposed methods for tract-based analysis of DTI/rsfMRI datasets of other brain diseases such as Alzheimer's disease and Autism. We envision that the proposed rsfMRI-guided fiber clustering approach could be a general methodology for tract-based fiber analysis in many brain conditions in the future.

Acknowledgments

T Liu was supported by the NIH Career Award EB 006878, NIH R01 HL087923-03S2, *NIH R01 R01DA033393, NSF CAREER Award IIS-1149260*, and The University of Georgia start-up research funding. B Ge was supported by the Fundamental Research Funds for the Central Universities from China (No. GK201001005). The authors would like to thank Carlos Faraco and L Stephen Miller for providing the working memory fMRI paradigm used in this paper. The SZ dataset was provided by the NA-MIC. *The authors would like to thank the anonymous reviewers for their constructive and helpful comments.*

References

Basser PJ, Pierpaoli C. Microstructural and physiological features of tissues elucidated by quantitative-diffusion-tensor MRI. Journal of Magnetic Resonance Series B. 1996; 111(3):209–219. [PubMed: 8661285]

Basser PJ, Pjevic S, Pierpaoli C, et al. In vitro fiber tractography using DT-MRI data. Magnetic Resonance in Medicine. 2000; 44(4):625–632. [PubMed: 11025519]

Behrens TEJ, Johansen-Berg H, Woolrich MW, smith SM, Wheeler-Kingshott CAM, Boulby PA, Barker GJ, Sillery EL, Sheehan K, Ciccarelli O, Thompson AJ, JM Brady, Matthews PM. Non-invasive mapping of connections between human thalamus and cortex using diffusion imaging. Nat Neurosci. 2003; 6(7):750–757. [PubMed: 12808459]

Behrens, Johansen-Berg H.; Robson, TEJ.; Drobnjak, MD.; Rushworth, I.; Brady, MFS.; Smith, JM.; Higham, SM.; Matthews, DJ. Changes in connectivity profiles define functionally distinct regions in human medial frontal cortex. proc Natl Acad Sci USA. 2004; 101:13335–13340. [PubMed: 15340158]

Brun, A.; Knutsson, H.; Park, HJ.; Shenton, ME.; Westin, CF. Clustering Fiber Traces Using Normalized Cuts; Proceedings of the 7th International Conference on Medical Image Computing and Computer-Assisted Intervention (MICCAI); 2004. p. 368-75.

Chen, Hanbo; Li, Kaiming; Zhu, Dajiang; Zhang, Tuo; Jin, Changfeng; Guo, Lei; Li, Lingjiang; Liu, Tianming. Inferring Group-wise Consistent Multimodal Brain Networks via Multi-view Spectral Clustering. MICCAI. 2012 in press.

Chen, Hanbo; Cai, Xiao; Zhu, Dajiang; Nie, Feiping; Liu, Tianming; Huang, Heng. Group-wise Consistent Parcellation of Gyri via Adaptive Multi-view Spectral Clustering of Fiber Shapes. MICCAI. 2012 in press.

Cohen, Alexander L.; Fair, Damien A.; Dosenbach, Nico UF.; Miezin, Francis M.; Donna, Dierker; David C, Van Essen; Schlaggar, Bradley L.; Petersen, Steven E. Defining functional areas in individual human brains using resting functional connectivity MRI. NeuroImage. 2008; 41(1):45–57. [PubMed: 18367410]

Corouge I, Gouttard S, Gerig G. Towards a Shape Model of White Matter Fiber Bundles Using Diffusion Tensor MRI. ISBI. 2004:344–347.

Downhill JE Jr, Buchsbaum MS, Wei T, Spiegel-Cohen J, Hazlett EA, Haznedar MM, Silverman J, Siever LJ. Shape and size of the corpus callosum in schizophrenia and schizotypal personality disorder. Schizophr Res. 2000 May; 42(3):193–208. [PubMed: 10785578]

Faraco CC, Unsworth N, Langley J, Terry D, Li K, Zhang D, Liu T, Miller LS. Complex span tasks and hippocampal recruitment during working memory. NeuroImage. 2011; 55(2):773–787. [PubMed: 21182968]

Fox MD, Raichle ME. Spontaneous fluctuations in brain activity observed with functional magnetic resonance imaging. Nat Rev Neurosci. 2007; 8:700–711. [PubMed: 17704812]

Frey BJ, Dueck D. Clustering by Passing Messages between Data Points. Science. 2007; 315:972–976. [PubMed: 17218491]

Friston K. Modalities, modes, and models in functional neuroimaging. Science. 2009; 326(5951):399–403. [PubMed: 19833961]

Ge B, Guo L, Li K, Li H, Faraco C, Zhao Q, Miller S, Liu T. Automatic Clustering of White Matter Fibers via Symbolic Sequence Analysis. SPIE Medical Image. 2010; 7623:762327.1–762327.8.

Ge, Bao; Guo, Lei; Hu, Xintao; Han, Junwei; Liu, Tianming. Resting state fMRI-guided fiber clustering. Medical Image Computing and Computer-Assisted Intervention (MICCAI). 2011

Gerig G, Gouttard S, Corouge I. Analysis of Brain White Matter via Fiber Tract Modeling. IEEE EMBS. 2004; 2:4421–4424.

Heuvel, van den Martijn; Mandl, Rene; Hulshoff Pol, Hilleke. Normalized cut group clustering of resting-state fMRI data. PLoS One. 2008; 3(4):e2001. [PubMed: 18431486]

Honey C, Sporns O, Cammoun L, Gigandet X, Thiran J, Meuli R, Hagmann P. Predicting human resting-state functional connectivity from structural connectivity. Proc Natl Acad Sci USA. 2009; 106(6):2035–2040. [PubMed: 19188601]

Innocenti GM, Ansermet F, Parnas J. Schizophrenia, neurodevelopment and corpus callosum. Molecular Psychiatry. 2003; 8:261–274. [PubMed: 12660799]

Kanaan RA, Kim JS, Kaufmann WE, Pearlson GD, Barker GJ, McGuire PK. Diffusion tensor imaging in schizophrenia. Biol Psychiatry. 2005 Dec 15; 58(12):921–9. [PubMed: 16043134]

Kerchner GA. Ultra-high field 7T MRI: a new tool for studying Alzheimer's disease. J Alzheimers Dis. 2011; (3):91–5. [PubMed: 21971453]

Kyriakopoulos M, Bargiotas T, Barker GJ, Frangou S. Diffusion tensor imaging in schizophrenia. Eur Psychiatry. 2008 Jun; 23(4):255–73. [PubMed: 18524546]

Kubicki M, McCarley R, Westin CF, Park HJ, Maier S, Kikinis R, Jolesz FA, Shenton ME. A review of diffusion tensor imaging studies in schizophrenia. J Psychiatr Res. 2007; 41(1-2):15–30. [PubMed: 16023676]

Li, K.; Guo, L.; Li, G.; Nie, J.; Faraco, C.; Zhao, Q.; Miller, S.; Liu, T. Cortical surface based identification of brain networks using high spatial resolution resting state FMRI data. ISBI; 2010. p. 657-659.

Hai, Li; Zhong, Xue; Lei, Guo; Tianming, Liu; Jill, Hunter; Stephen, Wong. A Hybrid Approach to Automatic Clustering of White Matter Fibers. NeuroImage. 2010; 49(2):1249–1258. [PubMed: 19683061]

Liu, Tianming; Shen, Dinggang; Davatzikos, Christos. Deformable Registration of Cortical Structures via Hybrid Volumetric and Surface Warping. NeuroImage. 2004; 22(4):1790–801. [PubMed: 15275935]

Liu, Tianming; Young, Geoffrey; Huang, Ling; Chen, Nan-Kuei; Wong, Stephen. 76-space Analysis of Grey Matter Diffusivity: Methods and Applications. Neuroimage. 2006; 15(31):51–65. [PubMed: 16434215]

Liu T, Li H, Wong K, Tarokh A, Guo L, Wong S. Brain Tissue Segmentation Based on DTI Data. NeuroImage. 2007; 38(1):114–23. [PubMed: 17804258]

Liu T, Nie J, Tarokh A, Guo L, Wong S. Reconstruction of Central Cortical Surface from MRI Brain Images: Method and Application. NeuroImage. 2008; 40(3):991–1002. [PubMed: 18289879]

Liu T. A few thoughts on brain ROIs, Brain Imaging and Behavior. 2011 in press.

Maddah M, Mewes AUJ, et al. Automated atlas-based clustering of white matter fiber tracts form DTMRI. MICCAI. 2005; 2005:188–195. [PubMed: 16685845]

Maddah M, Grimson W, Warfield S. Statistical Modeling and EM Clustering of White Matter Fiber Tracts. ISBI. 2006; 1:53–56.

Mezer A, Yovel Y, Pasternak O, Gorfine T, Assaf Y. Cluster analysis of resting-state fMRI time series. NeuroImage. 2009; 45(4):1117–25. [PubMed: 19146962]

Mori S, Crain BJ, Chacko VP, van Zijl PCM. Three dimensional tracking of axonal projections in the brain by magnetic resonance imaging. Annals of Neurology. 1999; 45(2):265–269. [PubMed: 9989633]

Mori S. Principles of Diffusion tensor imaging and its applications to basic neuroscience research. Neuron. 2006; 51(5):527–539. [PubMed: 16950152]

Nie, Jingxin; Guo, Lei; Li, Kaiming; Wang, Yonghua; Chen, Guojun; Li, Longchuan; Hanbo, Chen; Deng, Fan; Jiang, Xi; Zhang, Tuo; Huang, Ling; Faraco, Carlos; Zhang, Degang; Guo, Cong; Yap, Pew-Thian; Hu, Xintao; Li, Gang; Lv, Jinglei; Yuan, Yixuan; Zhu, Dajiang; Han, Junwei; Sabatinelli, Dean; Zhao, Qun; Miller, L Stephen; Xu, Bingqian; Shen, Ping; Platt, Simon; Shen, Dinggang; Hu, Xiaoping; Liu, Tianming. Axonal Fiber Terminations Concentrate on Gyri, accepted. Cerebral Cortex. 2011

O'Donnell LJ, Kubicki M, Shenton ME, Dreusicke MH, Grimson WE, Westin CF. A method for clustering white matter fiber tracts. AJNR Am J Neuroradiol. 2006; 27:1032–1036. [PubMed: 16687538]

O'Donnell LJ, Westin CF. Automatic tractography segmentation using a high-dimensional white matter atlas. IEEE Transactions on Medical Imaging. 2007; 26(11):1562–1575. [PubMed: 18041271]

Paul LK, et al. Agenesis of the corpus callosum: genetic, developmental and functional aspects of connectivity. Nat Rev Neurosci. 2007 Apr.8(4):288.

Rotarska-Jagiela A, Schönmeyer R, Oertel V, Haenschel C, Vogeley K, Linden DE. The corpus callosum in schizophrenia-volume and connectivity changes affect specific regions. NeuroImage. 2008; 39(4):1522–1532. [PubMed: 18096406]

Skudlarski P, Jagannathan K, Calhoun VD, Hampson M, Skudlarski BA, Pearlson GD. Measuring Brain Connectivity: Diffusion Tensor Imaging Validates Resting State Temporal Correlations. NeuroImage. 2008; 43:554–561. [PubMed: 18771736]

Tuch DS, Reese TG, Wiegell MR, Makris N, Belliveau JW, Wedeen VJ. High angular resolution diffusion imaging reveals intravoxel white matter fiber heterogeneity. Magn Res Med. 2002; 48(4):577–582.

Wakana S, Caprihan A, et al. Reproducibility of quantitative tractography methods applied to cerebral white matter. NeuroImage. 2007; 36:630–644. [PubMed: 17481925]

Westin CF, Maier SE, Mamata H, Nabavi A, Jolesz FA, Kikinis R. Processing and visualization of diffusion tensor MRI. Medical Image Analysis. 2002; 6(2):93–108. [PubMed: 12044998]

Xia Y, Turken U, Whitfield-Gabrieli SL, Gabrieli JD. Knowledge-based classification of neuronal fibers in entire brain. MICCAI. 2005; 3479:205–212. [PubMed: 16685847]

Zhang T, Guo L, Hu X, Li G, Nie J, Jiang X, Zhang D, Liu T. Joint analysis of fiber shape and cortical folding patterns. ISBI. 2010:1165–1168.

Zhang T, Guo L, Hu X, Li K, Jin C, Cui G, Li L, Liu T. Predicting Functional Cortical ROIs based on Fiber Shape Models. Cerebral Cortex. 2011 in press.

Zhang, Degang; Guo, Lei; Hu, Xintao; Li, Kaiming; Zhao, Qun; Liu, Tianming. Increased cortico-subcortical functional connectivity in schizophrenia, accepted. Brain Imaging and Behavior. 2011

Zhu, Dajiang; Li, Kaiming; Faraco, Carlos; Deng, Fan; Zhang, Degang; Jiang, Xi; Chen, Hanbo; Guo, Lei; Miller, Stephen; Liu, Tianming. Optimization of Functional Brain ROIs via Maximization of Consistency of Structural Connectivity Profiles. NeuroImage. 2011 in press.

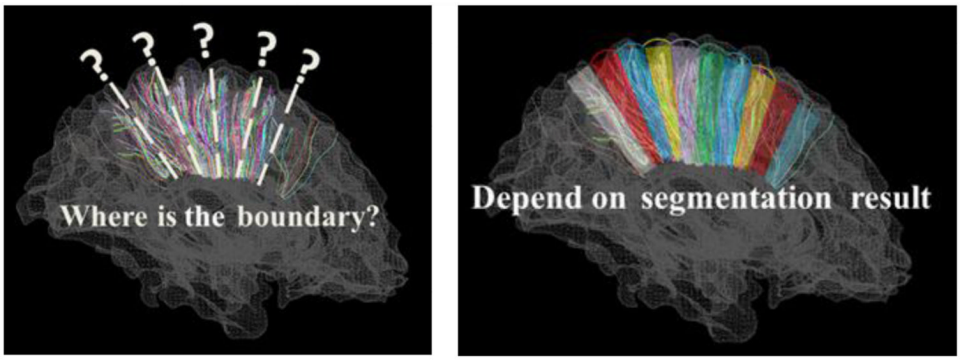

Fig.1.

Illustration of difficulties in fiber shape and end point based clustering methods. (a) Ambiguities in generating boundaries in shape based fiber clustering. (b) Uncertainty in fiber end point based clustering due to the reliance on cortical parcellation and recognition.

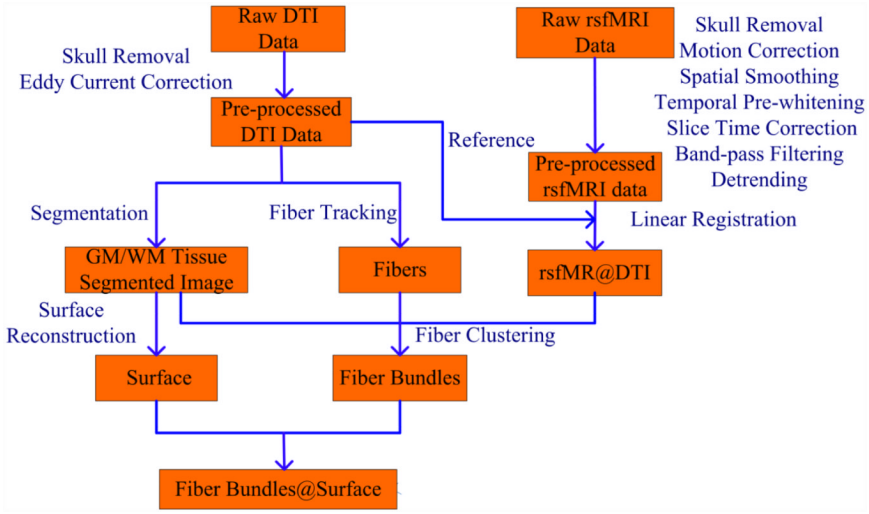

Fig.2.

The flowchart of our computational framework. It is noted that the DTI image space is used as the data analysis space.

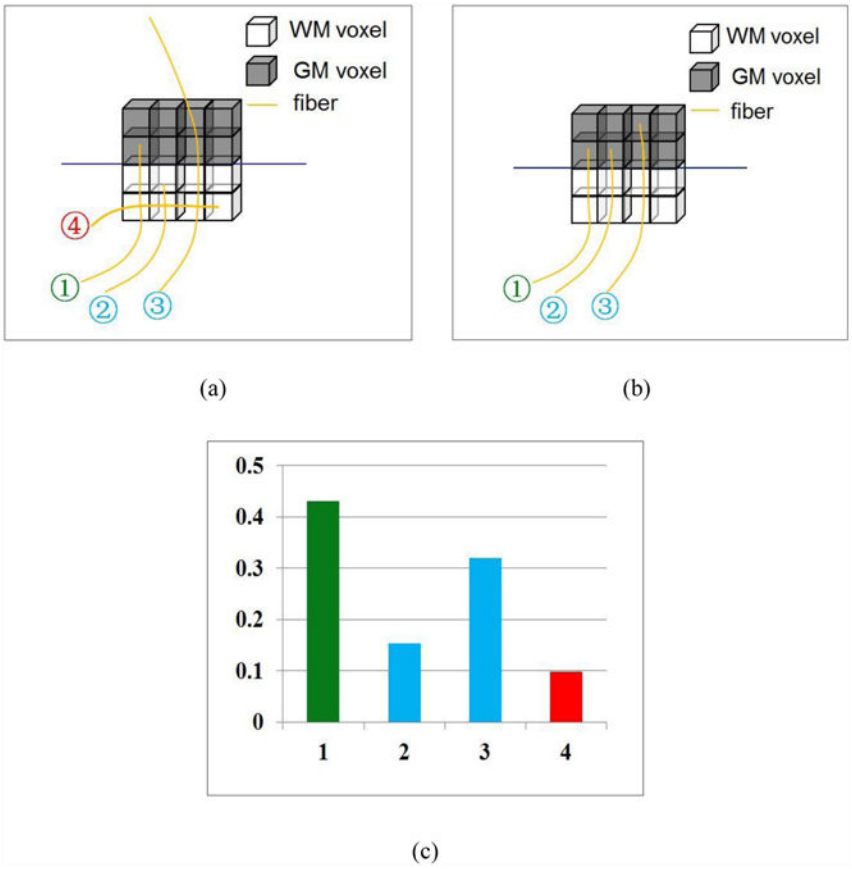

Fig.3.

Illustration of fiber projection. Gray matter and white matter voxels are represented by gray and white color boxes respectively. Fibers are represented by yellow curves. (a) The four situations before fiber projection; (b) The results of fiber projections for three situations. (c) The histogram of the four types of fibers in one randomly selected brain.

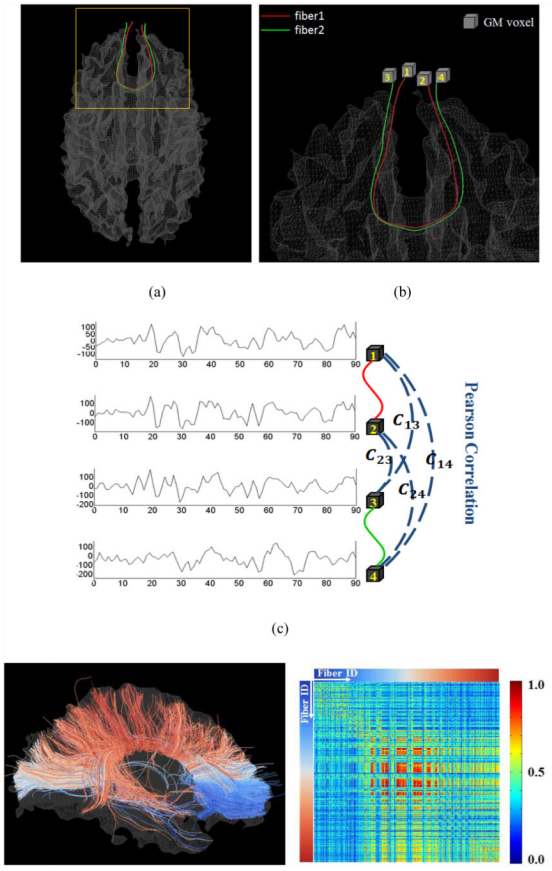

Fig.4.

The calculation of fibers' functional coherence. (a) Two fibers overlaid on the reconstructed cortical surface (gray mesh); (b) The zoomed-in view of the yellow rectangle in (a); (c) The rsfMRI signals of the four end points. Their correlations are measured by Eq. (1). (d) The color-coded fiber ID sequence; (e) The functional similarity matrix with a color bar of the similarity values on the right.

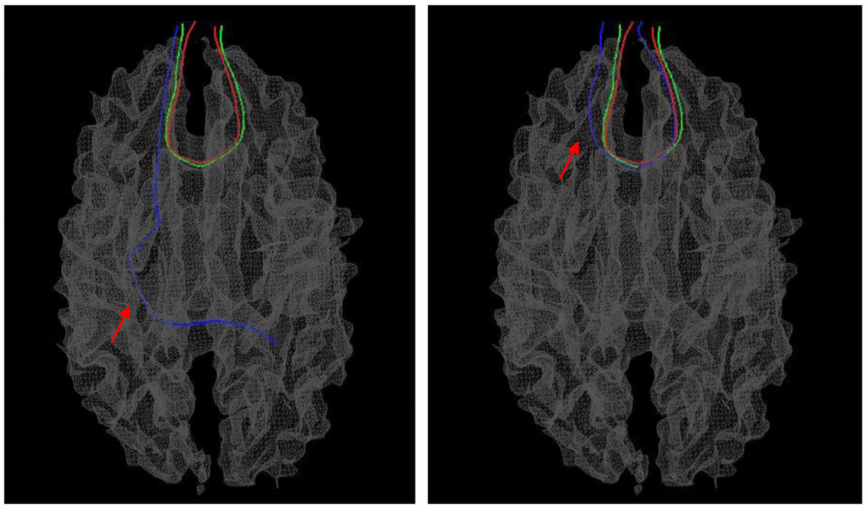

Fig.5.

(a) An example showing that functional coherence can cluster fibers of different shapes or geometries into the same bundle. (b) An example showing functional difference can differentiate neighboring fibers of similar shapes into different bundles.

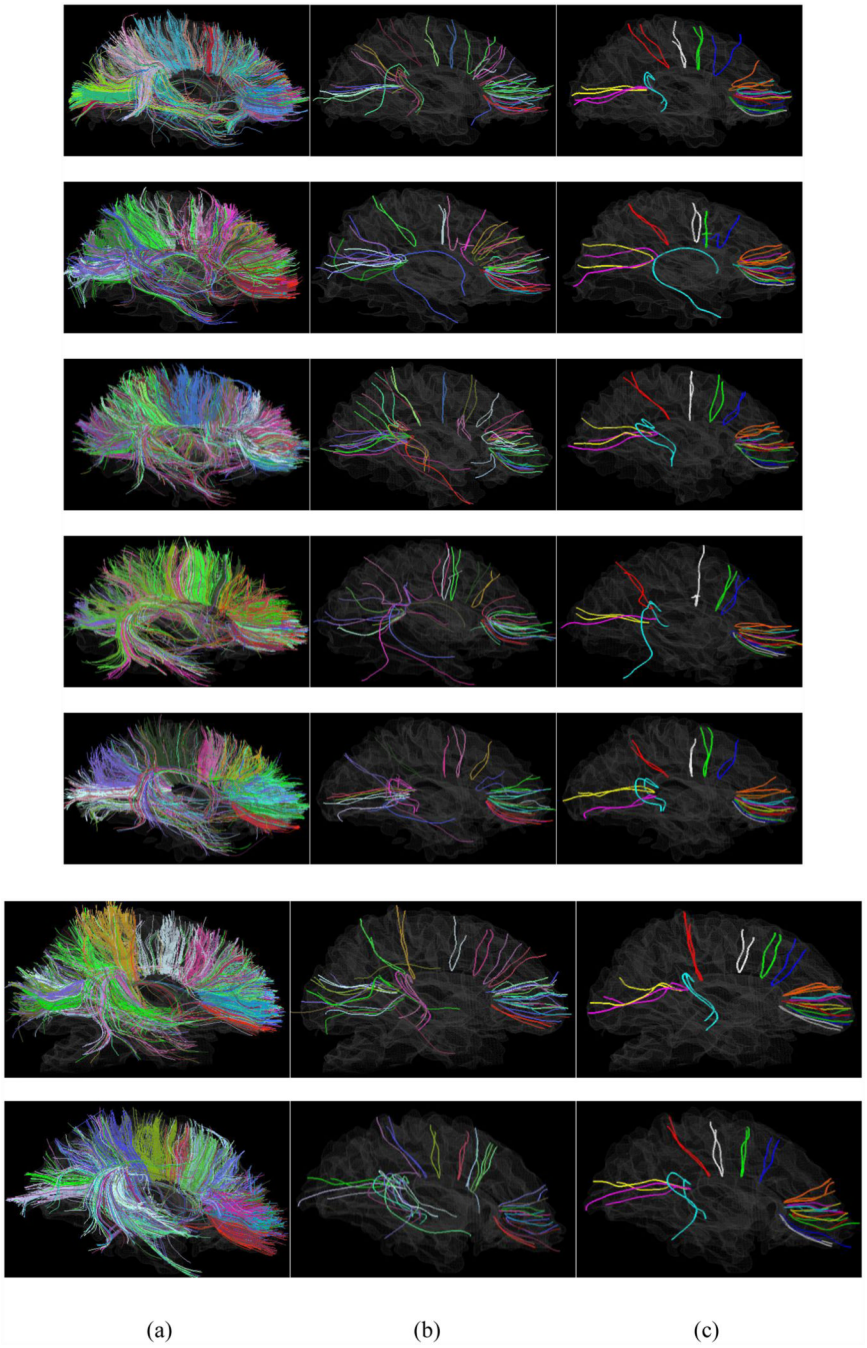

Fig.6.

The clustered fiber bundles for 7 subjects in 7 rows. (a) The fiber clusters with randomly set colors overlaid on the cortical surface; (b) The fiber exemplars of all clusters overlaid on the cortical surface. (c) The 16 most consistent fiber exemplars overlaid on the cortical surface. Each corresponding fiber exemplar has the same color in 7 different brains.

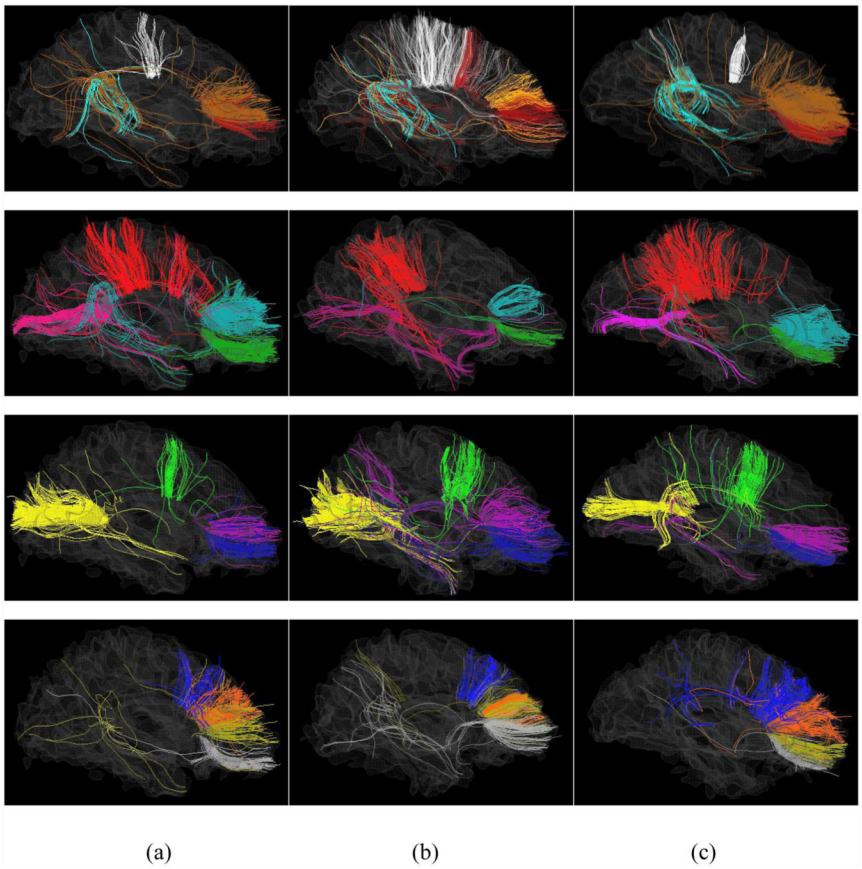

Fig.7.

Visualization of 16 corresponding fiber bundles from 3 randomly chosen subjects (three columns). They are labeled by the same colors as those in Fig. 6(c). Only 4 fiber bundles are shown in each figure for visual examination convenience. (a) 16 clustered fiber bundles of subject 1. (b) 16 clustered fiber bundles of Subject 2. (c) 16 clustered fiber bundles of Subject 3.

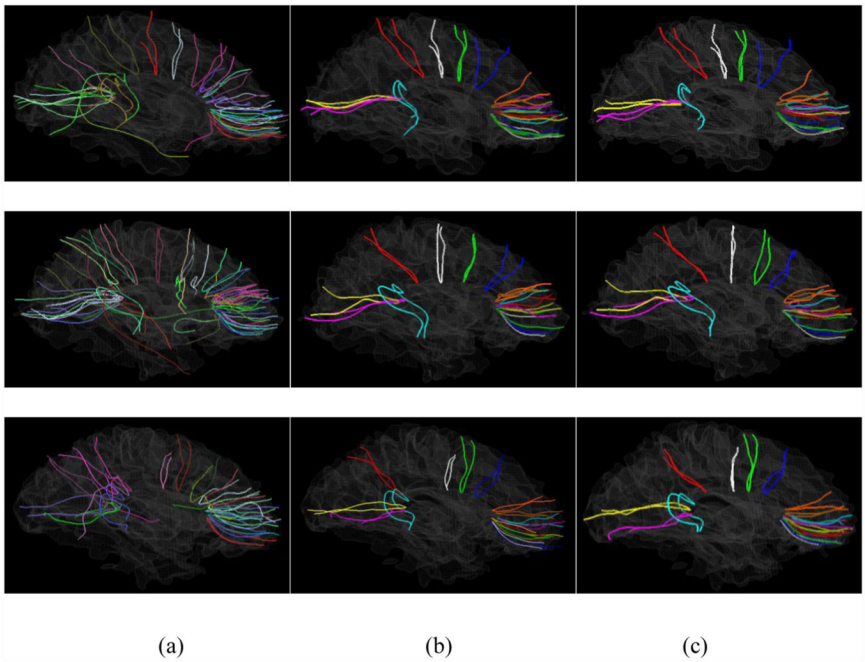

Fig.8.

The fiber clustering result from the repeated scans of rsfMRI data. (a) All exemplars. (b) 16 consistent exemplars. (c). The 16 consistent exemplars clustered in Fig. 6(c). The three rows correspond to #1, #3, and #5 rows of Fig. 6(c).

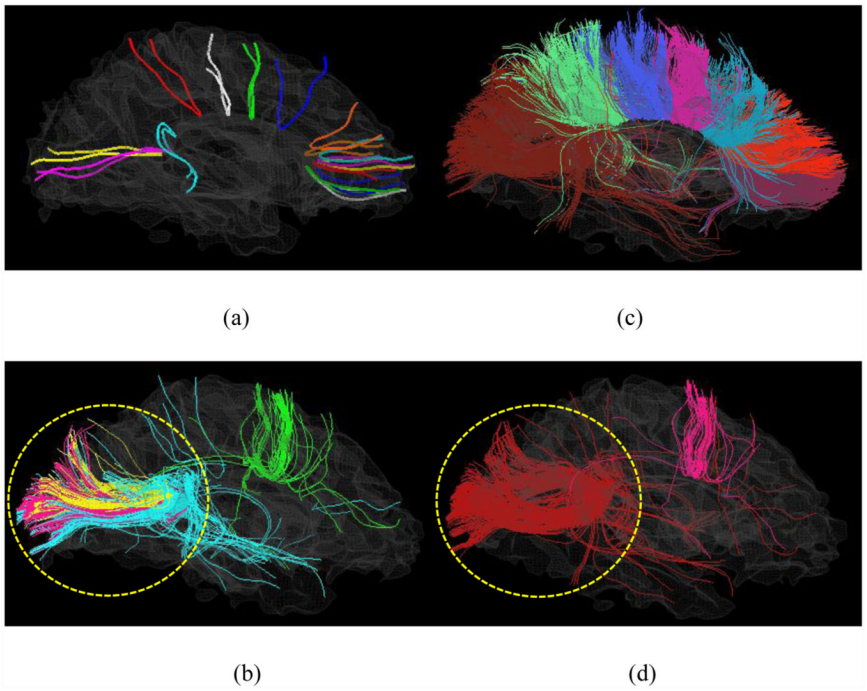

Fig.9.

The clustered fiber bundles by the two methods. (a) The 16 fiber exemplars overlaid on the cortical surface by our rsfMRI-guided fiber clustering method. (b) The 4 fiber bundles corresponding to the 4 selected exemplars in (a). (c) The 7 clustered fiber bundles overlaid on the cortical surface by shape based method. (d) The 2 clustered fiber bundles (that are exactly the fibers in (b)) by shape based method.

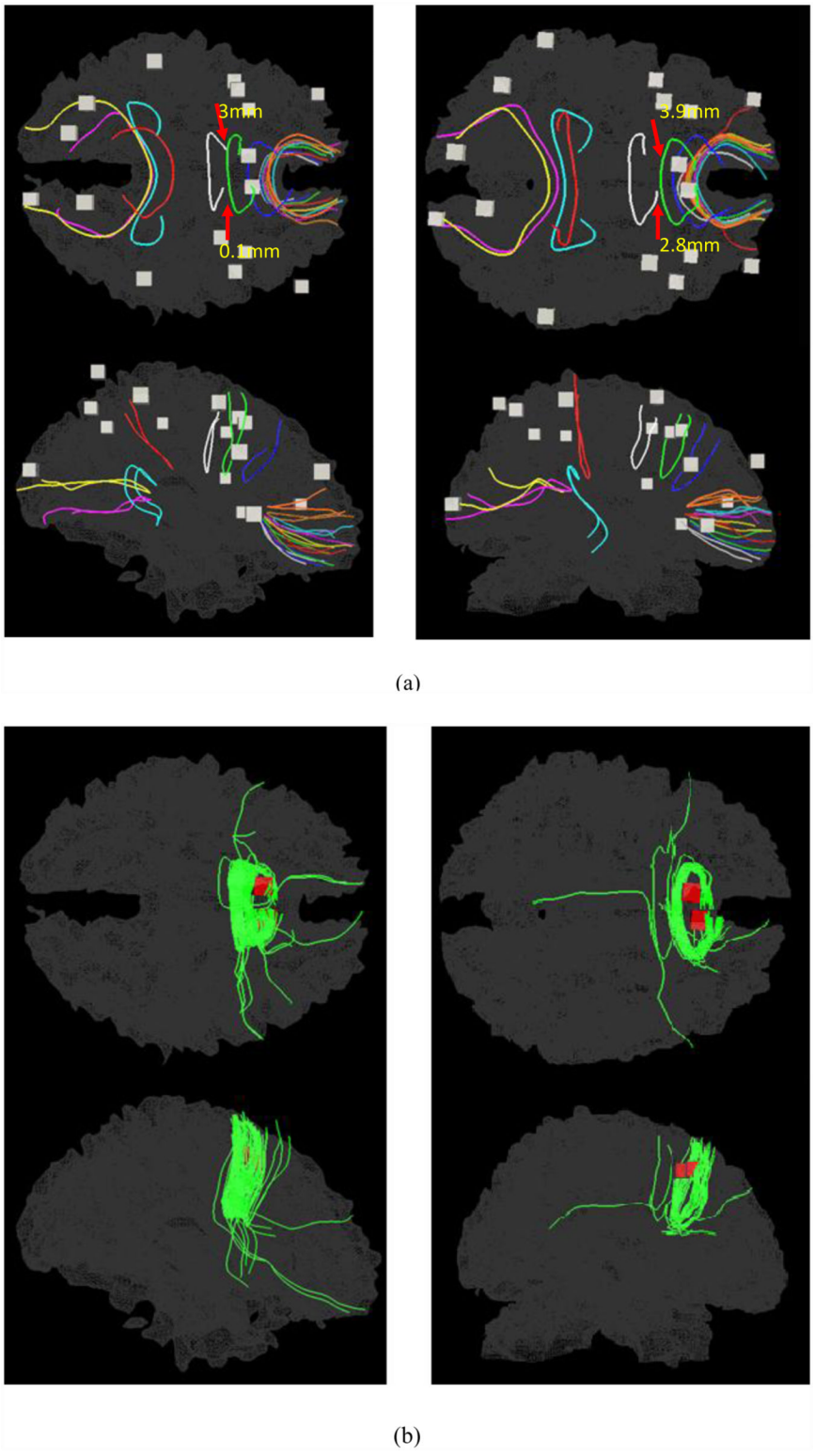

Fig.10.

(a) Joint visualization of 16 activated working memory ROIs (represented by green boxes) and clustered fiber bundles (represented by exemplars) for two subjects. The left and right

paracingulate gyri are connected by the corresponding blue fiber bundles. Each column shows two views of one subject. Two subjects are shown in two columns here. (b) The visualizations of fiber bundles corresponding to the two exemplars in green in (a).

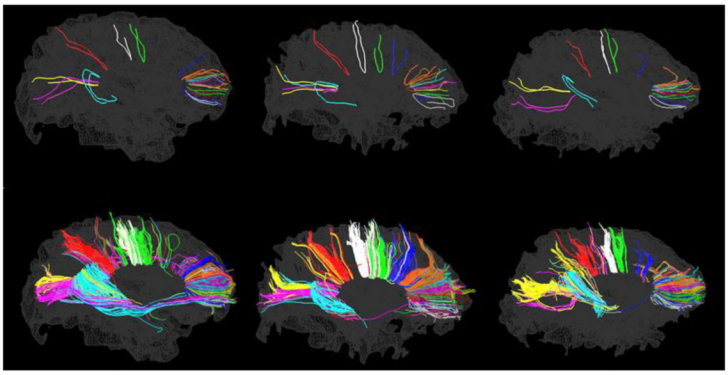

(a)

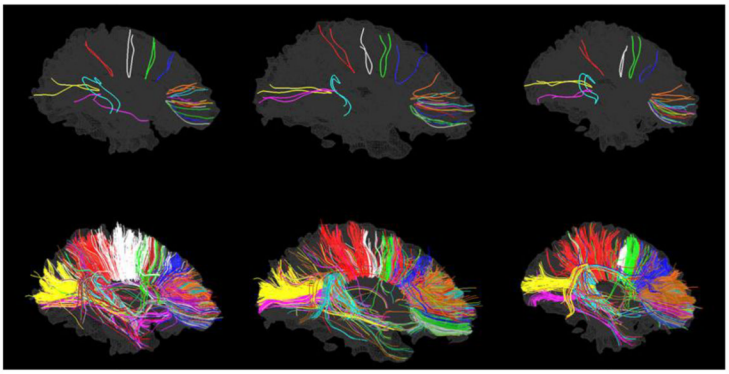

(b)

Fig.11.

The clustered fiber bundles and exemplars for randomly selected subjects including 3 SZ subjects and 3 controls. a) The 16 most consistent fiber bundles and exemplars of 3 SZ brains. (b) The 16 most consistent fiber bundles and exemplars of 3 controls overlaid on the reconstructed surfaces.

Table 1

Hausdorff distance between corresponding fiber bundles across pairs of different subjects (mm).

	Dis(s1,s2)	Dis(s1,s3)	Dis(s1,s4)	Dis(s1,s5)	Dis(s1,s6)	Dis(s1,s7)
1	7.4594	7.9382	6.5722	7.7377	10.5380	6.7594
2	6.8285	8.1507	14.427	9.3964	7.7484	5.6859
3	7.1926	7.8006	7.4426	4.9988	5.6172	4.8973
4	14.567	10.075	8.7182	11.096	8.0664	6.9811
5	10.666	7.9488	11.16	4.7918	3.1417	7.6074
6	7.4612	7.6013	8.9071	5.4789	7.748	4.9611
7	5.1965	4.6293	8.0429	7.5472	7.5621	6.7731
8	7.9188	9.326	12.005	7.2362	10.649	4.9601
9	6.8912	6.4566	4.53	3.7462	4.9518	4.9041
10	2.9481	7.535	7.821	4.5041	6.0299	6.5367
11	6.8644	8.7485	7.9698	8.3476	6.6369	6.5817
12	3.8157	5.5419	3.1686	5.2322	6.4253	6.7274
13	6.029	7.6148	6.7198	7.2049	5.399	7.1533
14	3.4143	4.6733	4.7041	4.5549	4.9052	7.4949
15	4.5497	5.6358	7.0846	4.5326	5.4704	5.5066
16	4.024	4.1635	4.0513	4.2563	3.237	5.5199

Table 2

Hausdorff distances (mm) between exemplars obtained in two repeated scans. 1: left-most fiber exemplar in Fig. 8(b); 16: right-most fiber exemplar in Fig. 8(b).

	Sbj1	Sbj3	Sbj5
1	0	0	7.4431
2	8.3516	0	6.9372
3	0	0.8739	0
4	0	0	10.9646
5	0	0	4.7673
6	1.9707	4.5989	0
7	0	8.3514	0
8	4.7973	1.8128	5.2194
9	2.3984	0	4.1409
10	4.5953	2.2751	0
11	5.6965	5.9833	3.6435
12	0	0	2.9992
13	7.7092	7.1107	3.0717
14	0	3.3693	4.2029
15	4.2637	3.9734	0
16	1.4934	4.7648	2.5956